Vol 10 No 1, January 2001
1009-1963/2001/10(01)/0046-06

Chinese Physics

©2001 Chin. Phys. Soc.
and IOP Publishing Ltd

MULTIPLE CLUSTER GROWTH OF ULTRA-THIN FILMS WITH ANISOTROPIC EDGE DIFFUSION*

WANG DAI-MU(王戴木)[a] and WU ZI-QIN(吴自勤)[b]

[a] *Department of Physics, Fuyang Teachers College, Fuyang 236032, China*

[b] *Department of Astronomy and Applied Physics, University of Science and Technology of China, Hefei 230026, China*

(Received 24 May 2000)

The multiple cluster growth of ultra-thin films on a hexagonal substrate with fractal, dendritic and compact morphology has been studied by computer simulation. The influence of the different diffusion processes along island edges on the island shape has been investigated. The results show that the anisotropic corner diffusion induces the dendritic growth, and the anisotropic step diffusion can promote the anisotropic growth and cause the ramified islands growing in three directions. In the case of compact growth, the island shape is mainly determined by the anisotropic corner crossing process. The nonuniform distribution of the multiple cluster formation can be described quantitatively by multifractal. With patterns changing from fractal to compact islands, the width and height of the bell-like or hook-like multifractal spectra increase, while the top $f(\alpha)$ decreases.

Keywords: thin film growth, computer simulation, multifractal
PACC: 6890, 0540

I. INTRODUCTION

Thin film growth processes are a subject of current interest.[1−4] Depending on the growth system and the deposition condition, islands formed during the early stages of growth exhibit morphologies which range from fractals to compact shapes. For example, by using scanning tunneling microscopy (STM), fractal and compact islands were observed for Pt on Pt(111),[5] dendritic islands were investigated for Ag on Pt(111),[6,7] and islands with needle-like shapes were found for Ag on a pseudomorphic monolayer of Ag adsorbed on Pt(111).[8] In order to explore the atomic nature of the kinetic mechanisms of the island growth, some growth simulations have been done.[8−13] Atomic processes important to island formation are diffusion of adatoms on terraces and along island edges. In addition, on fcc(111) surfaces two structurally different types of steps exist, and diffusion along these two steps can be different. Considering these factors, the kinetic Monte-Carlo (KMC) simulations can reproduce the fractal and dendritic islands observed in the experiment at low temperature.[8,11] However, at higher temperature the island growth is much complicated because many atomic processes are active simultaneously. It is not yet well understood how these anisotropic diffusion processes work together to control the island growth. In this paper, we simulate the growth processes of ultra-thin films in a wider temperature range. We pay special attention to the anisotropic edge diffusion, and investigate the influence of these diffusion processes on the island shape.

It has been suggested that multifractal can be used to account for some complex patterns and nonuniform distribution of physical parameters. In the past years, multifractal has been used to characterize ramified patterns observed by transmission electron microscopy (TEM),[14,15] rough surface measured by atomic force microscopy (AFM),[16] and secondary electron distributions simulated by Monte-Carlo method.[17,18] In order to describe quantitatively the subtle geometrical feature of the multiple cluster patterns of ultra-thin films, we analyse the cluster distributions by a multifractal approach.

II. SIMULATION

During deposition and growth, the adatom hops on the substrate at a rate of $h_s = \nu_s \exp(-E_s/kT)$, and hops along the edge with a rate $h_e = \nu_e \exp(-E_e/kT)$, where ν_s and ν_e are the attempt frequency for terrace and edge diffusion, and E_s and E_e the corresponding activation energy, respectively. The island shape (fractal or compact) is mainly determined by the ratio h_e/h_s. In Fig.1 we illustrate some important edge diffusion processes regarded here. There are three types of edge and corner diffusion: (1) corner

*Project supported by the Natural Science Foundation of Auhui Province, China (Grant No. 99047217).

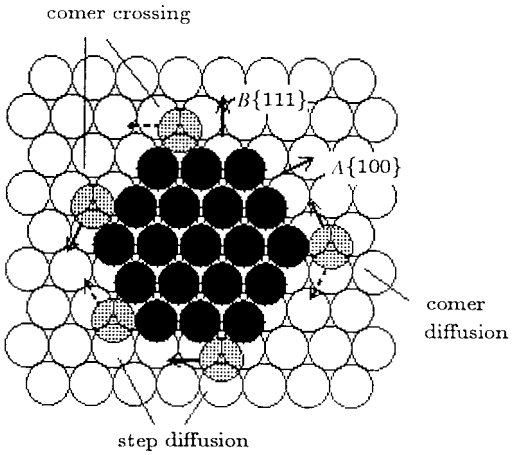


Fig.1. Illustrations of the various edge and corner diffusion processes. Dashed and full arrows indicate the diffusion via a top position and via channel position, respectively.

diffusion from 1-fold coordinated corner site to 2-fold step site; (2) corner crossing from 2-fold coordinated step site to 1-fold corner site; and (3) regular step diffusion (initial and final coordinations are 2). There are also two types of close-packed steps present on a hexagonal substrate: the B-steps with the {111}-facets and the A-steps with the more open {100}-facets[19] (see ball model in Fig.1). Our simulations use energy barriers (listed in Table 1) close to those calculated with the effective medium theory (EMT) for the system Ag/Pt(111).[8] According to the EMT calculation, the corner diffusion to A-step has an activation energy comparable to that obtained for terrace diffusion. Therefore, edge diffusion is active as soon as nucleation and aggregation set in. Assuming $\nu_s = \nu_e$, we get the ratio of edge diffusion rate to terrace diffusion rate at various substrate temperatures, as given in Table 2. Other rate processes such as the detachment of atoms from a step or the evaporation of adatom from an island are too slow in the given temperature range and have been ignored.

The multiple cluster growth of ultra-thin films generally include processes such as deposition, simultaneous diffusion of particles on the terrace, random nucleation and aggregation, and edge diffusion. We carried out the growth simulations on a hexagonal lattice containing 512×512 fcc sites with periodic boundary conditions. The model is described as follows: (1) particles are deposited successively with equal time interval W at randomly chosen site of the surface; (2) these deposited particles diffuse simultaneously along six directions with equal probability. Taking unit time as one diffusing step on terrace, the time interval W can be obtained as $W = h_s/R$, where R is deposition rate, i.e., an adatom can diffuse with W steps before the arrival of the next deposited atom; (3) if two particles meet at the nearest neighoring sites, they stop and form a nucleus. If a diffusing particle reaches the already formed clusters, the particle diffuses along the cluster edges according to h_e/h_s until it has at least three nearest neighbour particles belonging to the cluster.

Table 1. The energy barriers as calculated by the EMT for the system Ag/Pt(111) and used in the KMC simulations. E_s terrace diffusion, E_{cA} corner to A-step, E_{cB} corner to B-step, E_{Ae} and E_{Be} A- and B-step diffusion, E_{Ac} and E_{Bc} diffusion from A- and B-step to corner; all in unit of eV.

	E_s	E_{cA}	E_{cB}	E_{Ae}	E_{Be}	E_{Ac}	E_{Bc}
EMT	0.08	0.08	0.248	0.187	0.389	0.244	0.415
KMC	0.10	0.10	0.25	0.18	0.32	0.24	0.35

Table 2. Ratio of edge diffusion rate to terrace diffusion rate at various substrate temperatures.

	h_{cA}/h_s	h_{cB}/h_s	h_{Ae}/h_s	h_{Be}/h_s	h_{Ac}/h_s	h_{Bc}/h_s
80K	1	3.62×10^{-10}	9.22×10^{-6}	1.42×10^{-14}	1.00×10^{-9}	1.84×10^{-16}
150K	1	9.22×10^{-6}	2.06×10^{-3}	4.10×10^{-8}	2.00×10^{-5}	4.00×10^{-9}
240K	1	7.13×10^{-4}	2.10×10^{-2}	2.42×10^{-5}	1.16×10^{-3}	5.69×10^{-6}

The island density is determined by the diffusion steps W before the arrival of the next deposited atom, i.e., a high density of small islands is formed for small W, and a low density of large islands is obtained when W is large. In the growth simulations with T=80K, 150K, and 240K, we choose W=2×10^3 , 2×10^4 , and 1×10^5, respectively, relevant for a deposition rate of about 0.001–0.1 ML/s.

Ⅲ. RESULTS

Figure 2 shows a series of simulation patterns including fractal, dendritic, and compact islands for a fixed coverage ~0.15 monolayer (the total number of deposited particles $N = 4 \times 10^4$). In Fig.2(a), terrace diffusion is the only atomic displacements allowed. Atoms diffuse around on the surface until they irreversibly attach to the perimeter of a growing particle aggregate. The cluster growth is similar to the hit-and-stick diffusion limited aggregation (DLA) model. At 80K, the corner diffusion to an A-steps (the same process to B-steps is activated at higher temperature (see Table 2)) induces the dendritic islands with branches predominantly growing in three directions (Fig.2(b)). Increasing temperature to 150K, the diffusion process along A-steps becomes activated while the diffusion along B-steps is still frozen. The growth anisotropy leads to the islands with needle-like shape (Fig.2(c)). At this temperature, the anisotropic corner diffusion favors the growth in A-direction (see model Fig.1), and the anisotropic step diffusion enhances the anisotropic growth besides thickening the aggregates' branches. The effect is examined by the simulation in which we turn off the step diffusion anisotropy, i.e., set $E_{Be} = E_{Ae}$=0.18 eV, and the other parameters the same as Fig.2(c). The result presented in Fig.3 shows that compared with Fig.2(c) , now the growth along A-direction is less pronounced and the islands bear some of the irregular characteristic due to the symmetric step diffusion. Thus we can argue that at an intermediate temperature (150K) the anisotropic corner diffusion and step diffusion processes work together to control the islands growing in three directions.

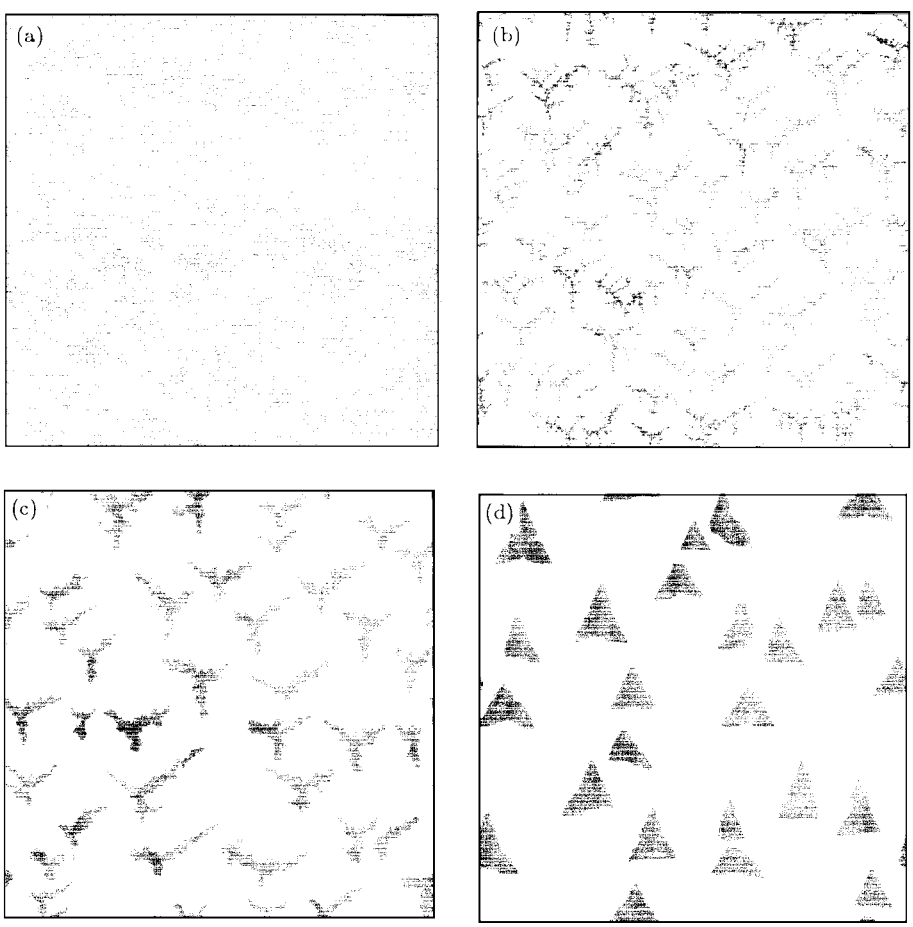


Fig.2. Multiple cluster patterns grown on hexagonal surface. The coverage is in all cases 0.15 ML. (a) hit-and-stick fractal growth, W=2×10^3; (b) dendritic growth, W=2×10^3, T=80K; (c) extremely anisotropic growth, W=2×10^4, T=150K; (d) compact islands, W=1×10^5 , T=240K. The energy barriers and relevant diffusion rates are listed in Table 1 and Table 2, respectively, the surface orientation is same as in Fig.1.

When the temperature reaches 240K, the corner crossing is active, the growing islands become compact. Owing to the larger difference between the energy barriers E_{Ac} and E_{Bc}, the diffusion from A-step via a corner to the B-step is much easier than that from a B-step via a corner to the A-step, and the adatoms will accumulate on the B-steps, thus the B-steps grow faster and disappear, resulting in the triangular islands with a different orientation (the tips point in B-direction)(Fig.2(d)). At this temperature the three types of edge and corner diffusion illustrated in Fig.1 are active simultaneously, but the anisotropic corner crossing overrides any effects due to anisotropic corner diffusion and step diffusion, and determines the shape of the compact islands.

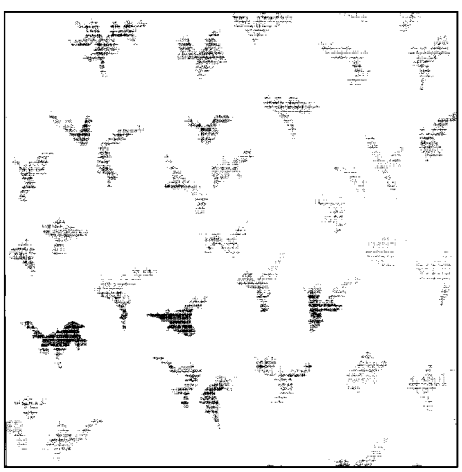


Fig.3. Growth simulation in which energy barrier E_{Be}=E_{Ae}=0.18eV, and all other parameters are the same as in Fig.2(c).

From Figs.2(b) and 2(c) , we can see that the anisotropy in corner diffusion is a strong effect at lower temperature. On the other hand, at higher temperature the anisotropic corner crossing plays dominant roles. In order to compare the kinetic effects of the two types of corner asymmetry, we equalize the corner diffusion and corner crossing energy barriers, i.e., set $E_{cA} = E_{Ac}$=0.24 eV and $E_{cB} = E_{Bc}$=0.35 eV, and turn off the step diffusion anisotropy. The simulation results are presented in Fig.4. In Fig.4(a), the corner crossing anisotropy is also turned off, the anisotropy in corner diffusion leads to the triangular islands surrounded by B-steps (the same orientation as those in Figs.2(b) and 2(c)). In Fig.4(c), the only asymmetry is the anisotropic corner crossing, now the growth leads to the inverted triangles exposing A-steps. When the two types of corner asymmetry are present, the anisotropic corner diffusion favors the A-steps growth, and the reverse process of anisotropic corner crossing favors the B-steps growth. The two effects compete with each other. The result is the hexagonal island shape, revealing both types of steps (Fig.4(b)). The

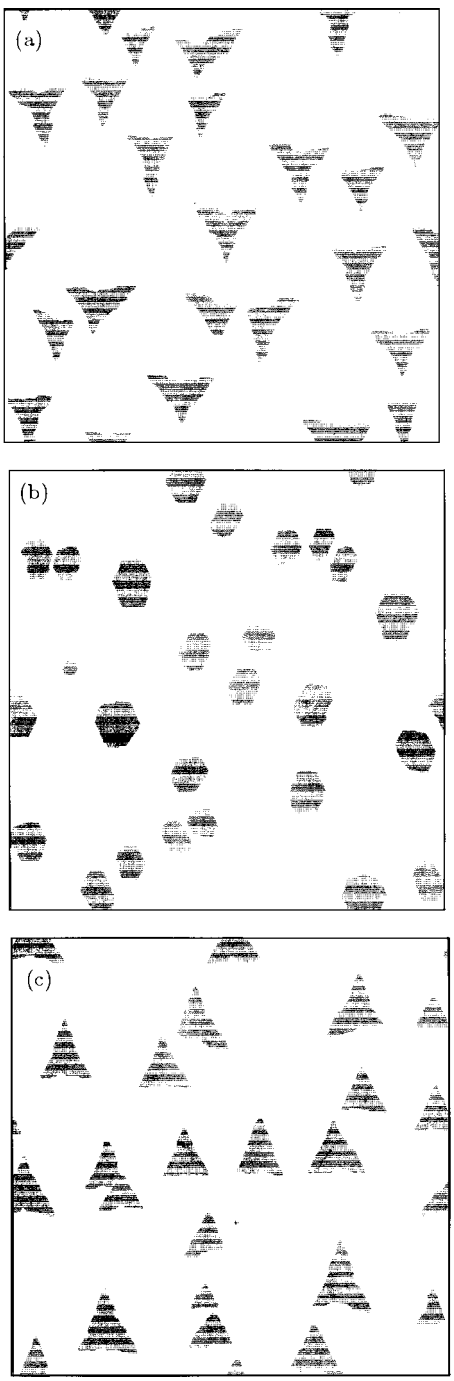


Fig.4. Influence of the corner asymmetry on the island shape. The step diffusion energy barriers are set to $E_{Be} = E_{Ae}$=0.18 eV, the corner diffusion and corner crossing energy barriers are: (a) E_{cA}/E_{cB}=0.24 eV/0.35 eV, E_{Ac}/E_{Bc}=0.24 eV/0.24 eV; (b) E_{cA}/E_{cB}=0.24 eV/0.35 eV, E_{Ac}/E_{Bc}=0.24 eV/0.35 eV; (c) E_{cA}/E_{cB} =0.24 eV/0.24 eV, E_{Ac}/E_{Bc}=0.24 eV/0.35 eV. The other parameters are the same as in Fig.2(d).

simulations show that in the case of compact growth, the island shape is determined by the relative strength of the two types of corner anisotropy. Of course, the anisotropic step diffusion can promote the growth in A-direction, but the asymmetry is not the main factor influencing the island shape. If the only asymmetry is the anisotropic step diffusion, the growth will lead to the triangular hexagons,[10,12] the sharp triangular islandslike those observed in the experiment cannot be obtained.

IV.MULTIFRACTAL ANALYSIS

To characterize quantitatively the nonuniform distribution of these ramified and compact islands, we investigate the multifractal behavior of the pattern formation and calculate the multifractal spectrum. Using the box-counting method the growth probability can be obtained as

$$P_{ij}(\varepsilon) = S_{ij}(\varepsilon)/\sum S_{ij}(\varepsilon), \tag{1}$$

where $S_{ij}(\varepsilon)$ is the number of particles inside a square box with a size of ε at position (i,j), and the $\sum S_{ij}(\varepsilon)$ is the summation over all the boxes. Let ε=1 when the total lattice of 512×512 sites is taken as the largest box, so that ε of smaller boxes is less than 1.

In the limit of small ε values, the following scaling relations are used,

$$P(\varepsilon) \sim \varepsilon^{\alpha}, \tag{2}$$

$$N_{\alpha}(\varepsilon) \sim \varepsilon^{-f(\alpha)}, \tag{3}$$

where α is the singularity, $N_{\alpha}(\varepsilon)$ the number of small squares of relative size ε with the same singularity. The multifractal spectrum $f(\alpha)$ can be obtained starting from a partition function $\chi_q(\varepsilon)$ defined as

$$\chi_q(\varepsilon) = \sum [P_{ij}(\varepsilon)]^q \sim \varepsilon^{\tau(q)}, \tag{4}$$

where q is the moment order and $\tau(q)$ the index of the power law. From $(q,\tau(q))$, one can compute $(\alpha, f(\alpha))$ by performing Legendre transformation.[20,21]

The multifractal spectra of the growth probability distribution corresponding to Fig.2 are presented in Fig.5, and the relevant parameters of the multifractal spectra are listed in Table 3, where $f(\alpha)_{\max}$ is the top $f(\alpha)$, i.e., Hausdorff dimension of the nonuniform distribution of the islands, the width of the spectra $\Delta\alpha = \alpha_{\max} - \alpha_{\min}$, the left-side height $\Delta f' = f(\alpha)_{\max} - f(\alpha_{\min})$, and the right-side height $\Delta f'' = f(\alpha)_{\max} - f(\alpha_{\max})$. From Fig.5 it is evident that with increasing temperature, the width and height of the multifractal spectra increase , while the top $f(\alpha)$ decreases. When the temperature is higher, $f(\alpha)_{\max}$ becomes less because there are larger vacant regions between nearby clusters. The minimum singularity $\alpha_{\min}$ and the maximum singularity $\alpha_{\max}$ are connected with the largest and smallest subsets of probability, respectively(Eq.(2)). With patterns changing from fractal to compact islands, the range of the bell-shaped or hook-shaped spectra $\Delta\alpha$ becomes wider, indicating that the difference between the largest and smallest subsets of probabilities becomes larger, and the growth probability distribution becomes more irregular and more nonuniform. The parameters $f(\alpha_{\min})$ and $f(\alpha_{\max})$ are the fractal dimension of the largest subset and smallest subset respectively. As the temperature increases, the number of branches of the clusters decrease rapidly, thus the smallest subset is associated with the smaller and smaller fractal dimension, leading to an asymmetric $f(\alpha)$ with the increasing right-side height of the hook-shaped spectra.

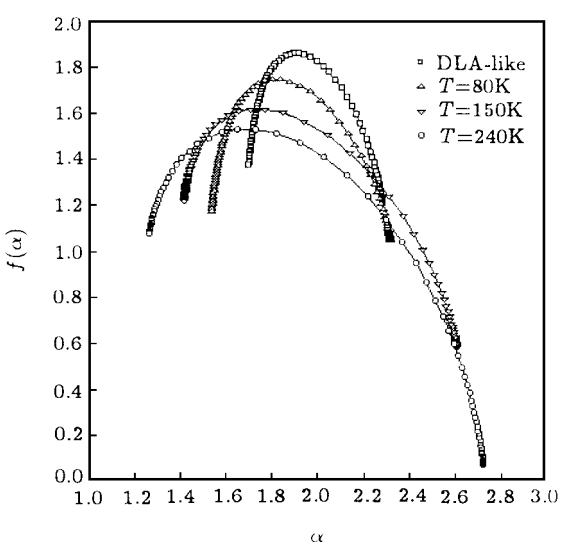


Fig.5. The multifractal spectra of multiple cluster growth in Fig.2.

Table 3. Parameters of the multifractal spectra shown in Fig.5.

	$\alpha_{\min}$	$\alpha_{\max}$	$\Delta\alpha$	$f(\alpha)_{\max}$	$f(\alpha_{\min})$	$f(\alpha_{\max})$	$\Delta f'$	$\Delta f''$
DLA-like	1.697	2.282	0.585	1.863	1.371	1.221	0.492	0.642
80K	1.534	2.317	0.783	1.748	1.168	1.047	0.580	0.701
150K	1.414	2.607	1.193	1.621	1.216	0.580	0.405	1.041
240K	1.262	2.724	1.462	1.533	1.074	0.073	0.459	1.460

As seen from Fig.2, the growing islands become more and more compact with increasing temperature. Although the shape of individual clusters is not fractal at higher temperature, the nonuniform distribution of the fat dendrites or compact islands with different sizes shows multifractal behavior.

V. SUMMARY

The multiple cluster growth of ultra-thin films at different substrate temperatures has been studied by KMC simulations. A rich range of morphologies from DLA-like fractals, to dendrites, and to compact islands has been generated by using realistic growth model. Our simulations show that the two types of corner asymmetry have quite strong effect on the island shape. At a low temperature (80K), the anisotropic corner diffusion induces the dendritic islands. At an intermediate temperature (150K), the anisotropic corner diffusion and step diffusion lead to the extremely anisotropic growth, i.e., the islands grow in three directions. At a high temperature (240K), the anisotropy in corner crossing is relatively strong, and becomes the main factor determining the shape of the compact islands. These multiple cluster patterns obtained under different growth conditions can be characterized quantitatively by the multifractal. The multifractal spectra provide detailed information about the nonuniform distribution of the islands.

REFERENCES

[1] Hwang R Q *et al* 1991 *Phys. Rev. Lett.* **67** 3279

[2] Zhang Z Y, Chen X, Lagally M G 1994 *Phys. Rev. Lett.* **73** 1829

[3] Brune H *et al* 1995 *Thin Solid Films,* **264** 230

[4] Zhang Z Y, Lagally M G 1997 *Science* **276** 377

[5] Michely T *et al* 1993 *Phys. Rev. Lett.* **70** 3943

[6] Brune H *et al* 1994 *Nature* **369** 469

[7] Roder H *et al* 1993 *Nature* **366** 141

[8] Brune H *et al* 1996 *Surf. Sci.* **349** L115

[9] Wang D M, Zhao Y D, Wu Z Q 1992 *J. Appl. Phys.* **71** 5904

[10] Liu S D *et al* 1993 *Phys. Rev. Lett.* **71** 2967

[11] Hohage M *et al* 1996 *Phys. Rev. Lett.* **76** 2366

[12] Jacobsen J *et al* 1996 *Surf. Sci.* **359** 37

[13] Wu F M *et al* 1998 *Chin. Phys. Lett.* **15** 916

[14] Huang L J *et al* 1989 *Phys. Rev.* **B40** 858

[15] Wang Mu *et al* 1998 *Phys. Rev. Lett.* **80** 3089

[16] Wang B, Wang Y, Wu Z Q 1995 *Solid State Commun.* **96** 69

[17] Li H, Ding Z J, Wu Z Q 1995 *Phys. Rev.* **B51** 13554

[18] Li H, Ding Z J, Wu Z Q 1996 *Phys. Rev.* **B53** 16631

[19] Wang S C *et al* 1991 *Phys. Rev. Lett.* **67** 2509

[20] Wang X P, Wu Z Q 1999 *Wuli*(*Physics*) **28** 342(in Chinese)

[21] Wang D M, Wu Z Q 2000 *Chinese Physics* **9** 368